


Cite this: *J. Mater. Chem. A*, 2018, 6, 840Received 20th October 2017
Accepted 17th December 2017

DOI: 10.1039/c7ta09242c

rsc.li/materials-a

Aqueous-solution synthesis of Na₃SbS₄ solid electrolytes for all-solid-state Na-ion batteries†Tae Won Kim, Kern Ho Park, Young Eun Choi, Ju Yeon Lee and Yoon Seok Jung *

Room-temperature-operable all-solid-state Na-ion batteries (ASNBS) using sulfide Na-ion solid electrolytes (SEs) are promising because of their potential for greater safety, lower cost, and acceptable performance. Despite extensive developments in the area of sulfide Na-ion SEs, their poor chemical stability and prospects for wet-chemical synthesis have been overlooked to date. Herein, the scalable synthesis of Na₃SbS₄ via aqueous-solution routes using precursors of Na₂S, Sb₂S₃, and elemental sulfur for ASNBS is described. With no concerns about the evolution of toxic H₂S gas, the aqueous-solution-synthesized Na₃SbS₄ exhibits high ionic conductivities (0.1–0.2 mS cm⁻¹ at 25 °C). Importantly, the homogeneity of the aqueous solutions enables the creation of uniform Na₃SbS₄ coatings on FeS₂, Fe₂S/Na–Sn ASNBS, employing the aqueous-solution-synthesized Na₃SbS₄ and the Na₃SbS₄-coated FeS₂ for the SE layer and positive electrode, respectively, demonstrate a high charge capacity of 256 or 346 mA h g⁻¹ with good reversibility at 30 °C, highlighting their potential for practical applications.

Safety concerns about conventional Li-ion batteries, which originate from their use of flammable organic liquid electrolytes, have led to a slow-down in their widespread adoption for large-scale energy-storage applications such as battery-driven electric vehicles and grid-scale energy storage.^{1,2} Moreover, the limited Li resources in the Earth's crust, combined with recent rapid rises in the price of the Li precursor (Li₂CO₃), as well as its geologically uneven distribution, are all serious challenges.³ Therefore, the replacement of Li⁺ ions with Na⁺ ions as the charge carrier, combined with the solidification of electrolytes manufactured from nonflammable inorganic materials, would be an ideal solution.^{4–6}

To date, there has been significant progress in the development of sulfide Li⁺ superionic conductors, such as

Li_{9.54}Si_{1.74}P_{1.44}S_{11.7}Cl_{0.3} (25 mS cm⁻¹)⁷ and argyrodite Li₆PS₅Cl (>1 mS cm⁻¹),⁸ and their application to composite-structured bulk-type all-solid-state Li-ion batteries.^{6,7,9} The promising levels of performance of bulk-type all-solid-state Li-ion batteries can be attributed to the excellent properties of sulfide materials: not only their high ionic conductivities but also their deformability that allows two-dimensional contact with active materials by application of a pressing process at room temperature, thus avoiding the deterioration that accompanies high-temperature sintering processes.⁶ Following these successes, the first report on the use of highly conductive sulfide Na-ion solid electrolytes (SEs), cubic Na₃PS₄ (0.2 or 0.46 mS cm⁻¹),⁴ led to extensive developments of new sulfide Na-ion SEs, e.g., 94Na₃PS₄·6Na₄Si₄ (0.74 mS cm⁻¹),¹⁰ Na₃PSe₄ (1.16 mS cm⁻¹),¹¹ Na_{2.9375}PS_{3.9375}Cl_{0.0625} (1 mS cm⁻¹),¹² and Na₃P_{0.62}As_{0.38}S₄ (1.46 mS cm⁻¹).¹³ However, most efforts to develop Li-ion and Na-ion SEs have overlooked the serious problem of poor chemical stability. Conventional sulfide SE materials containing phosphorus are not stable in air.^{5,6,9} They react not only with water in ambient air to produce toxic H₂S gas, but also with oxygen in dry air, which is a serious obstacle to their practical application.^{5,6,9} Moreover, the synthesis protocols for SE materials in most previous reports have been restricted to conventional methods such as solid-state reaction at high temperatures, as well as ball-milling.^{6,9}

Recently, our group reported on the development of new Li-ion and Na-ion SEs, namely, glass 0.4LiI–0.6Li₄SnS₄ (ref. 9) and tetragonal Na₃SbS₄,⁵ respectively. These phosphorus-free materials exhibited excellent stability in dry air. Especially, Na₃SbS₄ does not produce toxic H₂S gas when exposed to water. Moreover, both 0.4LiI–0.6Li₄SnS₄ and Na₃SbS₄ dissolve completely in methanol or water without any side reactions. It was demonstrated that the resulting solutions could be used to form SE coatings on active materials^{5,9,14} or to infiltrate conventional lithium-ion battery electrodes with SEs,¹⁵ providing a breakthrough in terms of electrochemical performance and practical applications. However, the aforementioned solution-processes still rely on the conventional synthetic protocol: the SEs are prepared by either a high-

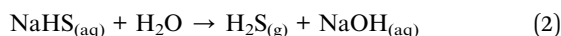
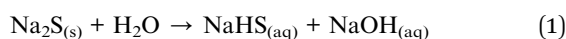
School of Energy and Chemical Engineering, Department of Energy Engineering, Ulsan National Institute of Science and Technology (UNIST), Ulsan 44919, South Korea.
E-mail: ysjung@unist.ac.kr

† Electronic supplementary information (ESI) available. See DOI: 10.1039/c7ta09242c

temperature solid-state reaction or by ball-milling prior to dissolution into the solvent.^{5,9,14,15} Although several results for the wet-chemical synthesis of Li-ion SEs using precursors such as Li₂S and P₂S₅ (e.g., Li₃PS₄ using tetrahydrofuran,^{16,17} Li₇P₂S₈I using acetonitrile,¹⁸ and Li₄PS₄I using dimethylethane¹⁹) have been reported, these solutions are not homogeneous, thus preventing their application to SE coatings or infiltration into the as-prepared electrodes.

Based on the above-mentioned research and motivations, we report on the application of the scalable synthesis of Na₃SbS₄ from a homogenous aqueous solution using precursors of Na₂S, Sb₂S₃, and elemental sulfur, for FeS₂/Na–Sn all-solid-state Na-ion batteries (ASNBs).

The processes for the aqueous-solution synthesis of Na₃SbS₄ are illustrated in Fig. 1a. Powdered Na₂S (twice the required amount), Sb₂S₃, and elemental sulfur are fully dissolved in deionized water, thus forming a homogeneous yellowish solution. The dissolution of Na₂S in water proceeds according to the following eqn (1) and (2).^{20,21}



It is suggested that the as-generated bisulfide anions (HS[−]) react with the Sb precursor, Sb₂S₃, generating a sulfur-rich anion, SbS₃^{3−}, as defined by eqn (3) and (4), which further reacts with the elemental sulfur to form SbS₄^{3−}, which is the building block for tetragonal Na₃SbS₄ (eqn (5)).²¹

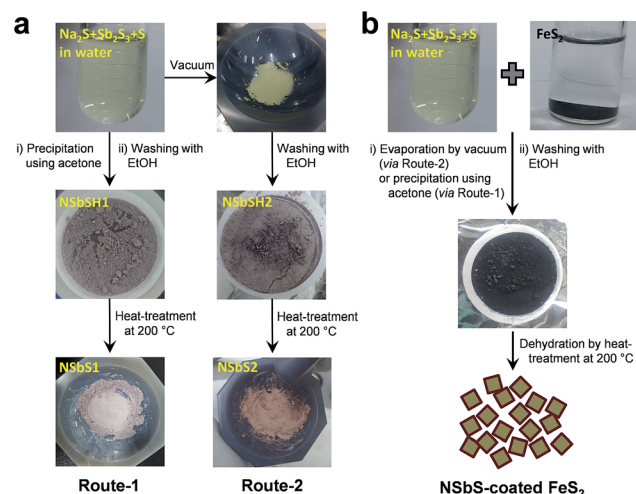
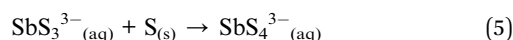
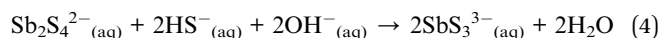
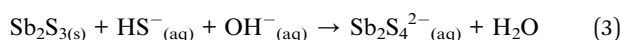


Fig. 1 Schematic illustrating (a) the synthesis of Na₃SbS₄ from aqueous solution using precursors of Na₂S, Sb₂S₃, and elemental sulfur and (b) its application to the coating of Na₃SbS₄ on the active material of FeS₂ powder.

The extraction of the Na₃SbS₄ from the as-prepared solutions was carried out *via* two different routes. For route-1, after the solids had been precipitated by adding acetone, the filtered powders were washed using ethanol to remove excess Na₂S and other impurities. The intermediate product is referred to as 'NSbSH1'.²⁰ From the thermogravimetric analysis (TGA) profile of NSbSH1, which exhibited a 26.2% weight loss below 100 °C and a constant value up to 400 °C (Fig. S1, ESI[†]), dehydration of the NSbSH1 was carried out by heat-treatment at 200 °C under vacuum, producing Na₃SbS₄ (NSbS1).²² For route-2, water in the solutions was evaporated under vacuum at room temperature. The subsequent procedure was the same as that for route-1. The as-developed synthetic routes applied for the Na₃SbS₄ coating onto the active material of FeS₂ are illustrated in Fig. 1b. Although the process *via* route-1 could be advantageous in terms of the preparation time, it suffers from severe evolution of H₂S gas during the precipitation using acetone (above 20 ppm, Fig. S2, ESI[†]). In contrast, the amount of H₂S gas evolved for the process *via* route-2 is controlled to be below 5 ppm under our experimental conditions, which would imply more practicality for route-2 than route-1 in terms of safety.²³

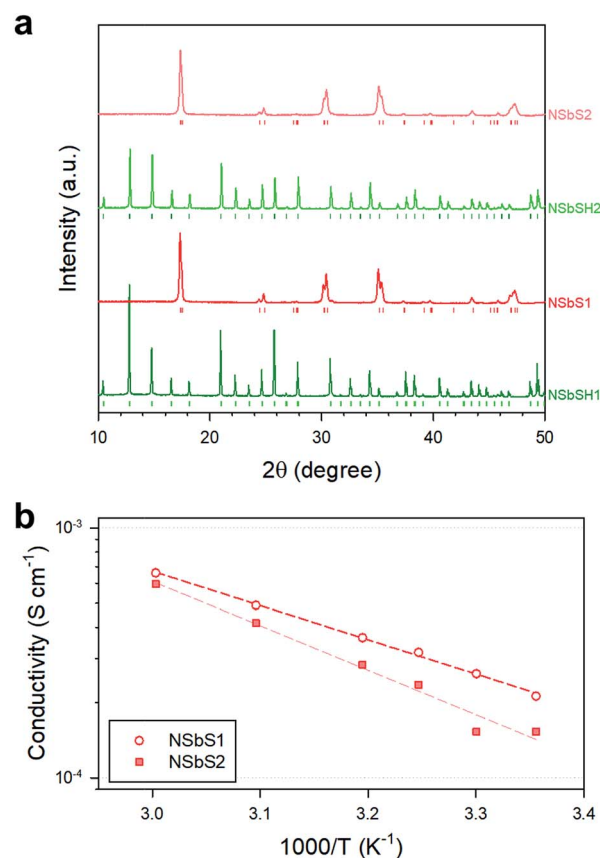


Fig. 2 (a) XRD patterns of the intermediate products (NSbSH1 and NSbSH2) and final products (NSbS1 and NSbS2) for the aqueous-solution synthesis of Na₃SbS₄. The Bragg positions of Na₃SbS₄·9H₂O (JCPDS no. 43-0442) and Na₃SbS₄ (ref. 5) are shown in green and red, respectively. (b) Arrhenius plots of Na-ion conductivities for the aqueous-solution-synthesized Na₃SbS₄.

The powder X-ray diffraction (XRD) patterns of the intermediate and final products of the aqueous-solution synthesis process are presented in Fig. 2a. While the intermediate products of NSbSH1 and NSbSH2 are isostructural with $\text{Na}_3\text{SbS}_4 \cdot 9\text{H}_2\text{O}$, the final products of NSbS1 and NSbS2 are identified as being tetragonal Na_3SbS_4 without any noticeable impurities.⁵ Fig. 2b shows the Arrhenius plots of the Na-ion conductivities measured by an AC impedance method using symmetric Ti/SE/Ti cells. NSbS1 and NSbS2 present similar conductivities at 25 °C (0.21 and 0.15 mS cm^{-1} , respectively) with activation energies of 0.27 and 0.35 eV, respectively. The conductivities of the aqueous-solution-synthesized Na_3SbS_4 are approximately one order of magnitude lower than that of the solid-state synthesized one (1.13 mS cm^{-1}), and similar to those of the one prepared in our previous work, by recrystallization from the solution in which the solid-state-synthesized Na_3SbS_4 is dissolved.⁵ The XRD patterns and conductivities of the aqueous-solution-synthesized Na_3SbS_4 heat-treated at different temperatures are also compared in Fig. S3, ESI.† By increasing the heat-treatment temperature from 200 to 400 or 550 °C, the XRD peaks were sharpened, indicating an increased level of crystallinity. However, the conductivities did not exhibit any notable enhancement: 0.25 mS cm^{-1} at 25 °C. The lower ionic conductivities of the aqueous-solution-synthesized Na_3SbS_4 , relative to that of the solid-state-synthesized one, can be attributed to the presence of impurities, such as antimony sulfides and oxides, associated with complex solution chemistries.⁵ Note that a conductivity of around 10^{-4} S cm^{-1} is a minimum requirement for the operation of all-solid-state batteries at moderately low C-rates (e.g., 0.1C) at room temperature.^{9,15} Further optimization of the aqueous-solution synthetic conditions may minimize the amount of impurities and thereby enhance the conductivities. Efforts to achieve this are underway.

We also attempted to extend the application of the aqueous-solution synthesis to a new structural class of SEs, namely, $\text{Na}_{4-x}\text{Sn}_{1-x}\text{Sb}_x\text{S}_4$ ($0.02 \leq x \leq 0.33$), which exhibits a maximum conductivity of 0.50 mS cm^{-1} at 30 °C ($\text{Na}_{3.75}\text{Sn}_{0.75}\text{Sb}_{0.25}\text{S}_4$) for the sample heat-treated at 550 °C.²⁴ The addition of the Sn precursor, SnS_2 , to Na_2S , Sb_2S_3 , and elemental sulfur in deionized water also resulted in complete dissolution, thus forming a homogeneous solution. Interestingly, the sample heat-treated at 200 °C consisted of Na_3SbS_4 and Na_4SnS_4 while heat-treatment at 550 °C resulted in a new phase of $\text{Na}_{3.75}\text{Sn}_{0.75}\text{Sb}_{0.25}\text{S}_4$ (Fig. S4, ESI†). This result may be explained by the difference in the solubility of the Sn and Sb species or by the meta-stability of the new phase at low temperatures. The aqueous-solution-synthesized $\text{Na}_{3.75}\text{Sn}_{0.75}\text{Sb}_{0.25}\text{S}_4$ heat-treated at 550 °C exhibited a high ionic conductivity of 0.23 mS cm^{-1} at 30 °C, which is comparable to that of its Na_3SbS_4 counterpart (0.29 mS cm^{-1} at 30 °C, Fig. S3b, ESI†).

FeS_2 was selected as an active material for producing Na_3SbS_4 coatings *via* the aqueous-solution synthesis routes because of its exceptional advantages: (i) low cost or abundance of raw material, (ii) excellent stability in water, which is in contrast to most conventional positive electrode materials for Na-ion batteries,²⁵ (iii) high theoretical capacity,^{26,27} and (iv) good electrical

conductivity.^{27,28} The XRD pattern and Raman spectrum of Na_3SbS_4 -coated FeS_2 prepared by the aqueous-solution process *via* route-2 are shown in Fig. 3a and b, respectively. The Raman spectra of the FeS_2 and the aqueous-solution-synthesized Na_3SbS_4 are also compared in Fig. 3b. The weight fraction of Na_3SbS_4 was determined to be 13 wt% from the measurements obtained using inductively coupled plasma optical emission spectroscopy (ICP-OES). The XRD peaks of tetragonal Na_3SbS_4 and cubic FeS_2 can be clearly seen with minor unknown impurity peaks (labeled '*'). Consistently, the characteristic bands of Na_3SbS_4 and FeS_2 are also observed in the Raman spectrum of Na_3SbS_4 -coated FeS_2 . However, a broad, low-intensity band centered at around 270 cm^{-1} can be seen, which is attributed to SbS_x impurities.⁵ In short, the XRD and Raman spectroscopy results confirm that the FeS_2 remains intact during the formation of Na_3SbS_4 *via* the aqueous-solution route, with negligible chemical reaction between the FeS_2 and Na_3SbS_4 .

Fig. 3c shows a field-emission scanning electron microscopy (FESEM) image of the Na_3SbS_4 -coated FeS_2 particle and its

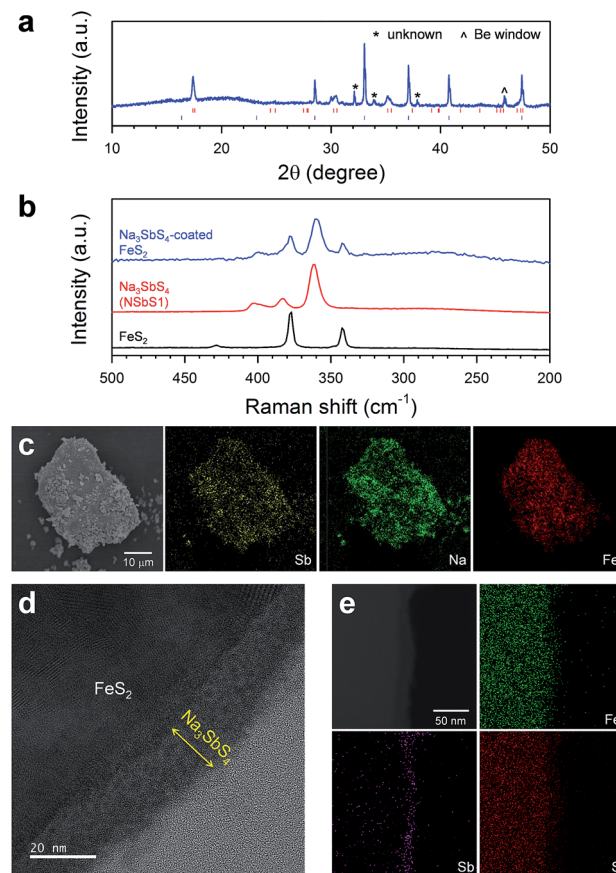


Fig. 3 Characterization of Na_3SbS_4 -coated FeS_2 prepared *via* the aqueous-solution route-2. (a) XRD pattern and (b) Raman spectrum of the Na_3SbS_4 -coated FeS_2 powder. The Bragg positions for Na_3SbS_4 (ref. 5) and FeS_2 (JCPDS no. 65-3321) are shown in red and violet, respectively, in (a). Raman spectra of aqueous-solution-synthesized Na_3SbS_4 and FeS_2 are compared in (b). (c) FESEM image of Na_3SbS_4 -coated FeS_2 and its corresponding elemental maps. (d) HRTEM and (e) scanning TEM images of the FIB-cross-sectioned Na_3SbS_4 -coated FeS_2 and EDXS elemental maps for the scanning TEM image.

corresponding energy dispersive X-ray spectroscopy (EDXS) elemental maps. The signals for the Sb and Na are distributed all over the particle, indicating good surface coverage of the Na_3SbS_4 coating layers. High-resolution transmission electron microscopy (HRTEM) images of the focused ion beam (FIB) cross-sectioned Na_3SbS_4 -coated FeS_2 particle and the corresponding Fast Fourier Transform (FFT) patterns are shown in Fig. 3d and S5, ESI†. It is seen that the approx. 20 nm tetragonal Na_3SbS_4 coating layer is in close contact with the cubic FeS_2 core, which is corroborated by the scanning TEM image and its corresponding elemental maps in Fig. 3e (another scanning TEM image and its corresponding elemental line profiles are shown in Fig. S6, ESI†).

Finally, $\text{FeS}_2/\text{Na-Sn}$ ASNBs were fabricated using the Na_3SbS_4 -coated FeS_2 (prepared *via* route-2) and Na_3SbS_4 (NSbS1) as the positive electrode and SE layer, respectively, and cycled between 0.6 and 3.0 V at $50 \mu\text{A cm}^{-2}$ and 30°C . Fig. 4a shows the first two-cycle discharge-charge voltage profiles where the discharge and charge capacities are 324 and 256 mA h g^{-1} , respectively. These values correspond to the uptake and extraction of 1.5 and 1.1 moles of Na, respectively. For up to 2 moles of Na, discharge (or sodiation) proceeds by a reversible intercalation reaction *via* the reduction of the sulfides.^{26,27} The cycling performance is shown in Fig. 4b. The $\text{FeS}_2/\text{Na-Sn}$ ASNBs retained 62% of their initial capacity after 50 cycles. This reversibility indicates good compatibility between FeS_2 and Na_3SbS_4 . Although lowering the cut-off voltage to 0 V could increase the capacity, capacity fading is expected due to severe volume changes resulting from the conversion reaction which proceeds *via* a reaction involving more than 2 moles of Na. $\text{FeS}_2/$

Na-Sn ASNBs employing Na_3SbS_4 -coated FeS_2 prepared *via* route-1 (17 wt% Na_3SbS_4) also showed high first-cycle discharge and charge capacities of 431 and 346 mA h g^{-1} , respectively (Fig. S7, ESI†).

In summary, a scalable aqueous-solution synthesis of Na_3SbS_4 using precursors of Na_2S , Sb_2S_3 , and elemental sulfur was successfully applied to ASNBs. The as-synthesized Na_3SbS_4 exhibited high ionic conductivities of $0.1\text{--}0.2 \text{ mS cm}^{-1}$ at 25°C . Importantly, it was demonstrated that the aqueous-solution route could be applied to high surface-coverage coating of Na_3SbS_4 on FeS_2 , which was attributed to the homogeneity of the solutions. Finally, $\text{FeS}_2/\text{Na-Sn}$ ASNBs employing Na_3SbS_4 -coated FeS_2 and Na_3SbS_4 , prepared *via* the aqueous-solution route, exhibited promising electrochemical performance. The simple process and the use of abundant (or low cost) and nontoxic elements/solvent should be emphasized when considering scalability and practical applications. Moreover, as confirmed by the extended application for the new class of SE $\text{Na}_{3.75}\text{Sn}_{0.75}\text{Sb}_{0.25}\text{S}_4$, the as-described solution synthesis has the potential to be applied to the production of new SE materials for practical all-solid-state technologies.

Conflicts of interest

There are no conflicts to declare.

Acknowledgements

This research was supported by the Technology Development Program to Solve Climate Changes of the National Research Foundation (NRF) funded by the Ministry of Science & ICT (No. 2017M1A2A2044501), and by the Materials and Components Technology Development Program of MOTIE/KEIT (10077709).

Notes and references

- 1 J. Kalhoff, G. G. Eshetu, D. Bresser and S. Passerini, *ChemSusChem*, 2015, **8**, 2154–2175.
- 2 A. Manthiram, X. Yu and S. Wang, *Nat. Rev. Mater.*, 2017, **2**, 16103.
- 3 N. Yabuuchi, K. Kubota, M. Dahbi and S. Komaba, *Chem. Rev.*, 2014, **114**, 11636–11682.
- 4 A. Hayashi, K. Noi, A. Sakuda and M. Tatsumisago, *Nat. Commun.*, 2012, **3**, 856.
- 5 A. Banerjee, K. H. Park, J. W. Heo, Y. J. Nam, C. K. Moon, S. M. Oh, S. T. Hong and Y. S. Jung, *Angew. Chem., Int. Ed.*, 2016, **55**, 9634–9638.
- 6 Y. S. Jung, D. Y. Oh, Y. J. Nam and K. H. Park, *Isr. J. Chem.*, 2015, **55**, 472–485.
- 7 Y. Kato, S. Hori, T. Saito, K. Suzuki, M. Hirayama, A. Mitsui, M. Yonemura, H. Iba and R. Kanno, *Nat. Energy*, 2016, **1**, 16030.
- 8 H. J. Deiseroth, S. T. Kong, H. Eckert, J. Vannahme, C. Reiner, T. Zais and M. Schlosser, *Angew. Chem., Int. Ed.*, 2008, **47**, 755–758.

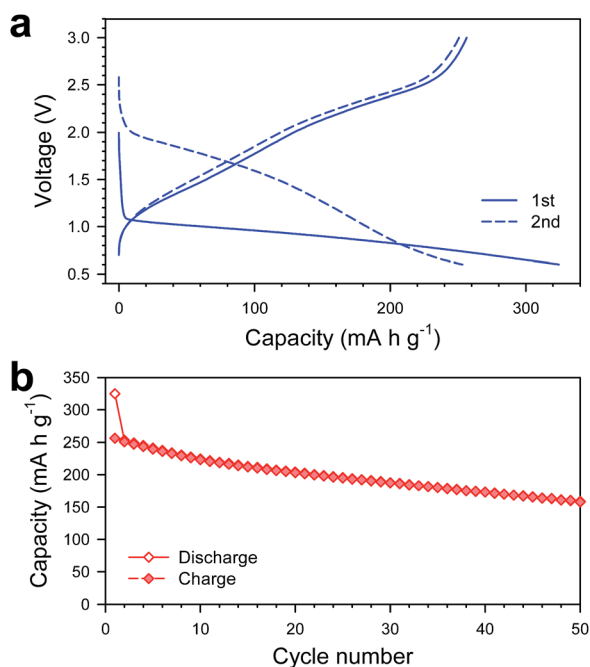


Fig. 4 Electrochemical performance of $\text{FeS}_2/\text{Na-Sn}$ ASNBs employing Na_3SbS_4 -coated FeS_2 prepared by the aqueous-solution process *via* route-2. (a) First two-cycle discharge-charge voltage profiles at $50 \mu\text{A cm}^{-2}$ and (b) the corresponding cycling performance.

- 9 K. H. Park, D. Y. Oh, Y. E. Choi, Y. J. Nam, L. Han, J. Y. Kim, H. Xin, F. Lin, S. M. Oh and Y. S. Jung, *Adv. Mater.*, 2016, **28**, 1874–1883.
- 10 N. Tanibata, K. Noi, A. Hayashi and M. Tatsumisago, *RSC Adv.*, 2014, **4**, 17120–17123.
- 11 L. Zhang, K. Yang, J. Mi, L. Lu, L. Zhao, L. Wang, Y. Li and H. Zeng, *Adv. Energy Mater.*, 2015, **5**, 1501294.
- 12 I. H. Chu, C. S. Kompella, H. Nguyen, Z. Zhu, S. Hy, Z. Deng, Y. S. Meng and S. P. Ong, *Sci. Rep.*, 2016, **6**, 33733.
- 13 Z. Yu, S. L. Shang, J. H. Seo, D. Wang, X. Luo, Q. Huang, S. Chen, J. Lu, X. Li, Z. K. Liu and D. Wang, *Adv. Mater.*, 2017, **29**, 1605561.
- 14 Y. E. Choi, K. H. Park, D. H. Kim, D. Y. Oh, H. R. Kwak, Y. G. Lee and Y. S. Jung, *ChemSusChem*, 2017, **10**, 2605–2611.
- 15 D. H. Kim, D. Y. Oh, K. H. Park, Y. E. Choi, Y. J. Nam, H. A. Lee, S. M. Lee and Y. S. Jung, *Nano Lett.*, 2017, **17**, 3013–3020.
- 16 Z. Liu, W. Fu, E. A. Payzant, X. Yu, Z. Wu, N. J. Dudney, J. Kiggans, K. Hong, A. J. Rondinone and C. Liang, *J. Am. Chem. Soc.*, 2013, **135**, 975–978.
- 17 D. Y. Oh, D. H. Kim, S. H. Jung, J.-G. Han, N.-S. Choi and Y. S. Jung, *J. Mater. Chem. A*, 2017, **5**, 20771–20779.
- 18 E. Rangasamy, Z. Liu, M. Gobet, K. Pilar, G. Sahu, W. Zhou, H. Wu, S. Greenbaum and C. Liang, *J. Am. Chem. Soc.*, 2015, **137**, 1384–1387.
- 19 S. J. Sedlmaier, S. Indris, C. Dietrich, M. Yavuz, C. Dräger, F. von Seggern, H. Sommer and J. Janek, *Chem. Mater.*, 2017, **29**, 1830–1835.
- 20 S. Ubaldini, F. Veglio, P. Fornari and C. Abbruzzese, *Hydrometallurgy*, 2000, **57**, 187–199.
- 21 B. Planer-Friedrich and N. Wilson, *Chem. Geol.*, 2012, **322–323**, 1–10.
- 22 H. Wang, Y. Chen, Z. D. Hood, G. Sahu, A. S. Pandian, J. K. Keum, K. An and C. Liang, *Angew. Chem., Int. Ed.*, 2016, **55**, 8551–8555.
- 23 <https://www.osha.gov/SLTC/hydrogensulfide/hazards.html>.
- 24 J. W. Heo, A. Banerjee, K. H. Park, Y. S. Jung and S.-T. Hong, *Adv. Energy Mater.*, DOI: 10.1002/aenm.201702716.
- 25 Z. Lu and J. R. Dahn, *Chem. Mater.*, 2001, **13**, 1252–1257.
- 26 A. Kitajou, J. Yamaguchi, S. Hara and S. Okada, *J. Power Sources*, 2014, **247**, 391–395.
- 27 Y. Xiao, S. H. Lee and Y.-K. Sun, *Adv. Energy Mater.*, 2017, **7**, 1601329.
- 28 Y. H. Liu, L. Meng and L. Zhang, *Thin Solid Films*, 2005, **479**, 83–88.